

Bifurcation analysis of the transition to turbulence in high symmetric flow

Lennaert van Veen, Kyoto University, Department of Mechanical Engineering
Email: veen@mech.kyoto-u.ac.jp

March 2, 2004

Abstract

Two scenarios leading to chaos and turbulence in high symmetric flow are described. Exploiting the symmetries and the divergence free condition the number of degrees of freedom, and thereby the computational effort, is reduced by a factor of about 300 compared to general direct simulation of fluid flow. This allows for bifurcation analysis at the transition points. At the first transition a sequence of torus doublings leads to temporal chaos, but the flow doesn't become turbulent. At lower viscosity the Ruelle-Takens scenario is followed and we are at the onset of turbulence. Some differences between these transitions are discussed in the light of bifurcation theory of invariant tori.

1 Introduction

Direct numerical simulation of flows at high Reynolds number requires solving large systems of differential equations. For the solutions to be realistic the smallest resolved spatial scale should be of the same order as the typical size of the smallest vortices, a few times Kolmogorov's dissipation scale. As the total number of degrees of freedom scales as the cube of the ratio of the largest to the smallest resolved scale the limitations of memory size and computation time are soon met. One way around this problem is to impose spatial symmetries on the solutions.

In the absence of boundaries the incompressible Navier-Stokes equations are invariant under translations (\mathbb{R}^3), rotations ($SO(3)$) and reflections (\mathbb{Z}_2^3). In Kida (1985) a subgroup of symmetries consisting of three finite rotations and three reflections is imposed on the solutions in a periodic box. In terms of finite truncations in Fourier space this reduces the number of independent modes by a factor of about 200. The resulting flow displays fully developed turbulence for low viscosity, whereas only a few hundred degrees of freedom are necessary to capture spatial scales small enough for reliable simulation. High symmetric flow was subsequently used to explore the statistics of turbulent motion at moderate Reynolds numbers (Kida & Murakami, 1989) and to find evidence for the Ruelle-Takens (1971) scenario at the transition from regular to chaotic motion Kida *et al.* (1989).

In the latter paper a combination of forward time integration and power spectra was used to study the transitions. Three-periodic motion was shown to occur as an intermediary state between quasi periodic and aperiodic motion. This was shown to happen at least

twice. At high viscosity temporal chaos ensues but the velocity profile remains simple. At lower viscosity vortices on small scales develop and turbulence sets in. In this work we will take a closer look at the bifurcation scenarios leading to chaos and turbulence, focusing on the differences between the transitions at high viscosity and low viscosity.

Using bifurcation analysis, Poincaré sections and power spectra we show that at high viscosity a sequence of torus doubling bifurcations leads to chaos. Beyond this transition the behaviour alternates between periodic, quasi periodic and chaotic for small variations of viscosity. Reducing viscosity further we find an interval with stable periodic motion and then a second transition to chaos. Here, the Ruelle-Takens scenario is followed. Beyond this transition point the flow starts to look turbulent as small scale vortices develop. The behaviour near the transition points is discussed in the light of bifurcation theory of invariant tori as presented in Broer *et al.* (1990).

2 The vorticity equation for high symmetric flow

Consider an incompressible fluid in a periodic box $0 < x_1, x_2, x_3 \leq 2\pi$. In terms of the Fourier representation of velocity and vorticity,

$$\mathbf{v} = i \sum_{\mathbf{k}} \tilde{\mathbf{v}}(\mathbf{k}) e^{i\mathbf{k}\cdot\mathbf{x}} \quad \boldsymbol{\omega} = \sum_{\mathbf{k}} \tilde{\boldsymbol{\omega}}(\mathbf{k}) e^{i\mathbf{k}\cdot\mathbf{x}} \quad (1)$$

we have

$$\frac{d}{dt} \tilde{\omega}_i(\mathbf{k}) = \epsilon_{ijk} k_j k_l \tilde{v}_k \tilde{v}_l - \nu k^2 \tilde{\omega}_i(\mathbf{k}) \quad k_i \tilde{u}_i = 0 \quad \tilde{\omega}_i(\mathbf{k}) = -\epsilon_{ijk} k_j \tilde{v}_k(\mathbf{k}) \quad (2)$$

where ν is the kinematic viscosity and the tilde denotes the Fourier transform. In terms of the standard norm energy and enstrophy are given by

$$E = \frac{1}{2} \|\mathbf{v}\|^2 \quad Q = \frac{1}{2} \|\boldsymbol{\omega}\|^2 \quad (3)$$

respectively.

Now consider the following discrete symmetry operations: S_i , reflections in the planes V_i given by $x_i = \pi$ and R_i , rotations over $\pi/2$ radians about the lines $l_i : x_j = \pi/2$ for $j \neq i$. The periodic domain with planes of reflection axes of rotation is shown in figure (1). Suppose the x -component of the velocity field is given in the box $[0, \pi/2] \times [0, \pi/2] \times [0, \pi/2]$. Applying the symmetry operation $R_2 \circ R_3$ yields the y -component and $(R_2 \circ R_3)^{-1}$ the z -component in that box. Subsequently $R_1, R_1^2, R_1^3, R_2^2, R_2^3, R_3^3$ and $R_1^2 \circ R_3$ yield the velocity field on the box $[0, \pi] \times [0, \pi] \times [0, \pi]$ and finally the reflections $S_1, S_2, S_2 \circ S_1, S_3, S_1 \circ S_3, S_2 \circ S_3$ and $S_1 \circ S_2 \circ S_3$ fill up the whole periodic domain. Thus only one out of three components in a volume fraction $1/4^3$ determines the whole flow, which reduces the computational effort by a factor 192. The divergence free condition is more conveniently handled in Fourier space.

Symmetry operations S_i and R_i introduce linear relations between the Fourier components of vorticity. First of all we have

$$\tilde{\omega}_1(k_1, k_2, k_3) = \tilde{\omega}_2(k_3, k_1, k_2) = \tilde{\omega}_3(k_2, k_3, k_1) \quad (4)$$

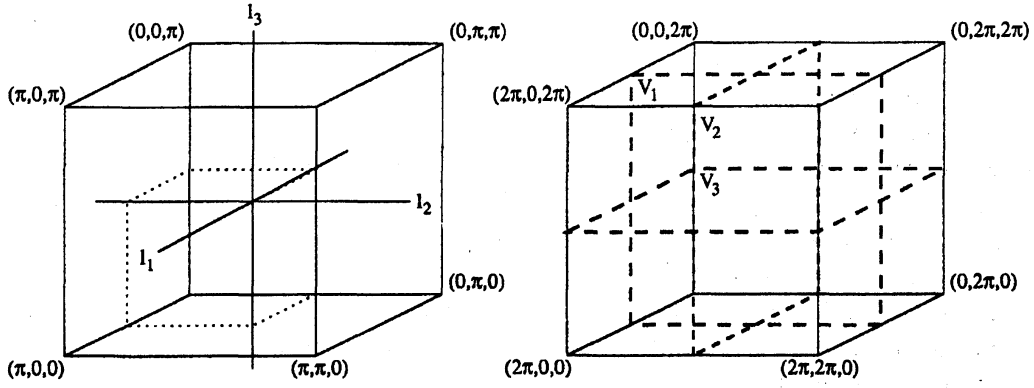


Figure 1: Left: the domain $[0, \pi] \times [0, \pi] \times [0, \pi]$ with the axes of rotation $l_{1,2,3}$ drawn in. Right: the domain $[0, 2\pi] \times [0, 2\pi] \times [0, 2\pi]$ with the planes of reflection $V_{1,2,3}$ drawn in. If one component of the vorticity field is specified in the box delimited by the dotted line, the full field on the periodic domain follows from symmetry.

so that we may consider only one component. This scalar function is even or odd in its arguments:

$$\tilde{\omega}_1(k_1, k_2, k_3) = \tilde{\omega}_1(-k_1, k_2, k_3) = -\tilde{\omega}_1(k_1, -k_2, k_3) = -\tilde{\omega}_1(k_1, k_2, -k_3) \quad (5)$$

and finally we have

$$\tilde{\omega}_1(k_1, k_2, k_3) = \begin{cases} -\tilde{\omega}_1(k_1, k_3, k_2) & \text{for } k_1 \text{ and } k_2 \text{ and } k_3 \text{ even,} \\ \tilde{\omega}_1(k_1, k_3, k_2) & \text{for } k_1 \text{ and } k_2 \text{ and } k_3 \text{ odd,} \\ 0 & \text{otherwise.} \end{cases} \quad (6)$$

We consider a cubic truncation, i.e. $|k_{1,2,3}| \leq N$. Relations (4)-(6) reduce the number of independent Fourier modes of vorticity by a factor of 192 in the leading order, that is N^3 . There is, however one more linear relation which allows for further reduction, namely the divergence free condition for vorticity. With the aid of relation (4) it reads

$$k_1 \tilde{\omega}_1(k_1, k_2, k_3) + k_2 \tilde{\omega}_1(k_2, k_3, k_1) + k_3 \tilde{\omega}_1(k_3, k_1, k_2) = 0 \quad (7)$$

Taking maximal advantage of relations (4)-(7) we consider only Fourier components of ω_1 in the fundamental domain $\{\mathbf{k} \in \mathbb{Z}^3 | k_3 > k_2, k_3 \geq k_1, k_1 \geq 0, k_2 > 0, k_3 \leq N\}$. A sketch of this domain is shown in figure (2). The number of independent modes is reduced by a factor of 288 in the leading order. These components satisfy the following equation

$$\begin{aligned} \frac{d}{dt} \tilde{\omega}_1(k_1, k_2, k_3) = & k_2 k_3 (\tilde{S}(k_3, k_1, k_2) - \tilde{S}(k_2, k_3, k_1)) + k_1 k_2 \tilde{T}(k_2, k_3, k_1) \\ & - k_3 k_1 \tilde{T}(k_3, k_1, k_2) + (k_2^2 - k_3^2) \tilde{T}(k_1, k_2, k_3) - \nu k^2 \tilde{\omega}_1(k_1, k_2, k_3) \end{aligned} \quad (8)$$

where \tilde{S} and \tilde{T} are the Fourier transforms of

$$S(x_1, x_2, x_3) = v_1(x_1, x_2, x_3)^2 \quad T(x_1, x_2, x_3) = v_1(x_2, x_3, x_1)v_1(x_3, x_1, x_2) \quad (9)$$

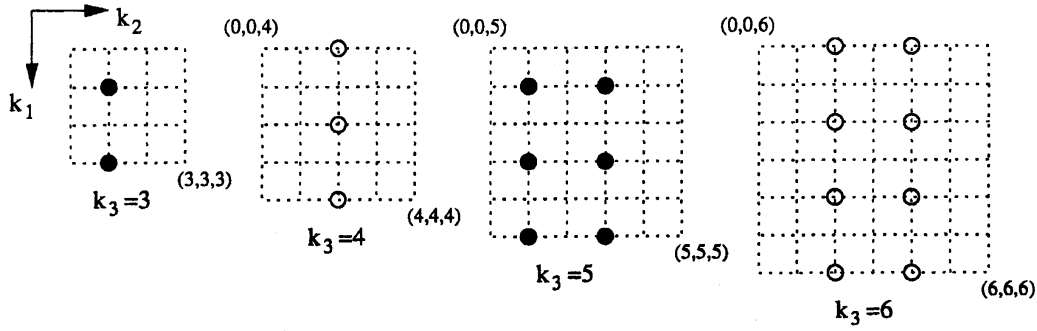


Figure 2: Wave vectors corresponding to independent amplitudes $\tilde{\omega}_1(\mathbf{k})$. Shown are the first four levels in k_3 , starting at the smallest wave vector $\mathbf{k} = (1, 1, 3)$. Solid: odd sub lattice. Open: even sub lattice.

and

$$k^2 \tilde{v}_1 = k_2 \tilde{\omega}_1(k_3, k_1, k_2) - k_3 \tilde{\omega}_1(k_2, k_3, k_1) \quad (10)$$

Energy is supplied by fixing the low order odd mode $\tilde{\omega}_1(1, 1, 3) = -3/8$. Thus we obtain a family of dynamical systems with one parameter, ν , and a number of degrees of freedom given by

$$n(N) = \begin{cases} \frac{2}{3} \left(\frac{N}{2}\right)^3 + \frac{1}{2} \left(\frac{N}{2}\right)^2 - \frac{7}{6} \frac{N}{2} & \text{if } N \text{ is even} \\ \frac{2}{3} \left(\frac{N-1}{2}\right)^3 + \frac{3}{2} \left(\frac{N-1}{2}\right)^2 - \frac{1}{6} \left(\frac{N-1}{2}\right) & \text{if } N \text{ is odd.} \end{cases} \quad (11)$$

3 Numerical considerations

In performing time integrations we avoid the use of the pseudo-spectral method commonly employed for three dimensional simulations. Due to the reduction of the number of degrees of freedom the direct method is not much slower and yields a simple, transparent code and easy access to the Jacobian for integration of the linearised system. The code is composed of two parts. First, all nonlinear interaction coefficients are computed for a given truncation level N . This is done by looping over all resonant triads for a given Fourier component and mapping all resonant modes onto the fundamental domain by symmetries (4)-(6) and relation (7). This process takes up to a few minutes for truncation levels up to $N = 21$, the highest resolution considered in Kida *et al.* (1989). After that a seventh to eighth order Runge-Kutta-Felbergh scheme with step size adjustment is employed for integration. The use of a high order method might seem odd for such large systems but as it turns out that the step size adjustment more than makes up for the larger number of evaluations of the vector field, 13 compared to 4 for fourth-order Runge-Kutta.

The following experiment was done to check this. If we do not fix $\tilde{\omega}_1(1, 1, 3)$ in time and set $\nu = 0$ kinetic energy E is conserved. The fourth-order and high order Runge-Kutta method were employed to integrate the conservative system over an interval Δt much larger than the typical time scale of fluctuations, which is $O(1)$. The error tolerance for the energy conservation was fixed to ϵ . For the high order method this is done by specifying the local error tolerance, for the low order method by choosing a small enough step size. For realistic $O(1)$ levels of the energy, $\Delta t \approx 10^3$ and $\epsilon = 10^{-9}$ it is found that

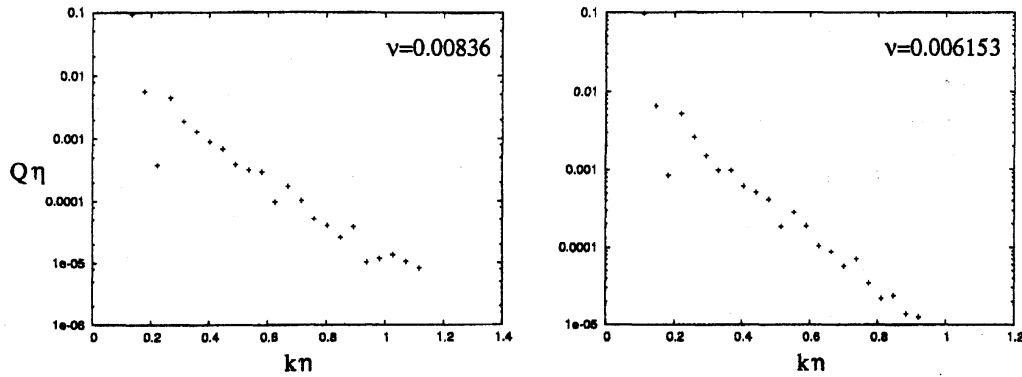


Figure 3: Band-averaged enstrophy spectra near the transitions to chaos (see section (4)). Obtained from an integration of 10^3 time units, log-linear scale in normalised units. Left: at the first transition, II \rightarrow III in figure (4). Right: at the second transition, V \rightarrow VI.

the average step size of the high order method is about ten times the required step size of the low order method. As many of the results presented here are based on rather long time integrations it is important to keep the error tolerance low. The seventh to eighth order Runge-Kutta-Felbergh scheme has been shown to be extremely reliable, see for instance Tuwankotta & Quispel (2003), where this scheme is shown to be as accurate as, albeit slower than, problem-specific symplectic methods in a nearly integrable problem.

Below simulations are performed with a viscosity in the range $0.004 < \nu < 0.01$ and the truncation level fixed to $N = 15$. We computed the energy and the enstrophy, as well as Taylor's micro-scale Reynolds number, R_λ , and Kolmogorov's dissipation length scale, η , defined by

$$R_\lambda = \sqrt{\frac{10}{3}} \frac{E}{\nu \sqrt{Q}}, \quad \eta = \sqrt[4]{\frac{\nu^2}{2Q}} \quad (12)$$

As a rule of thumb the ratio $\eta \|k\|_{max}$ has to be $O(1)$ for the truncation error to be negligible. In the viscosity range explored here it varies in the range $1.3 > \eta \|k\|_{max} > 0.63$. To make sure the truncation level is high enough to describe the transitions to chaos, the focus of this research, we computed the band-averaged enstrophy spectra at the transition points. They are shown in figure (3). At the small scales an exponential decay is visible, indicating that our numerical results are reliable. The time average micro-scale Reynolds number varies from $R_\lambda \approx 55$ to $R_\lambda \approx 27$, indicating that on the lower end of the viscosity scale we are at the onset of turbulence.

In addition to time integration we applied numerical bifurcation analysis to this system. For this end we use the software package AUTO (Doedel *et al.*, 1986). This software is not designed to handle large systems and a scaling needs to be introduced for computation of the determinant of the Jacobian (Doedel, 2003).

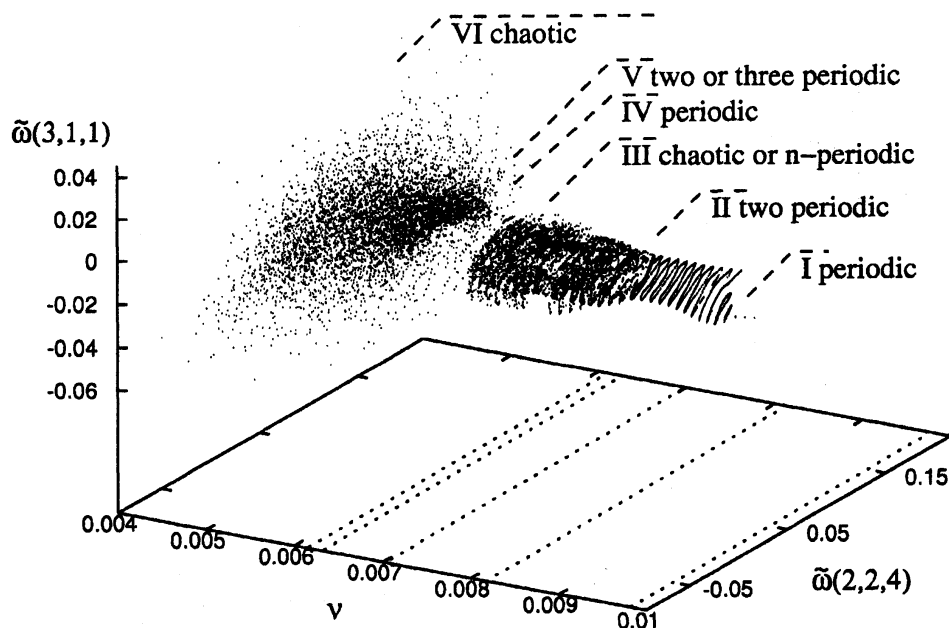


Figure 4: Limit point diagram in the range $0.01 > \nu > 0.004$. Visible is the transition I→II from periodic to quasi periodic, II→III to chaotic, III→IV back to periodic, IV→V to quasi periodic and V→VI to chaotic/turbulent. In region III the behaviour alternates between chaotic and two or three periodic while the spatial structure of the flow remains simple.

4 Transitions to chaos and turbulence

The focus of the present paper is the transition from regular to chaotic and turbulent behaviour for decreasing viscosity. In Kida *et al.* (1989) two and three periodic motion was found which implies that the Ruelle-Takens scenario is followed. It was also shown that, after an initial transition to temporal chaos regular (periodic) motion sets in. After a second transition the spatial behaviour becomes more complicated and turbulence develops. That work was mainly based on forward time integration, power spectra and measurement of the micro scale Reynolds number. In addition to these instruments we employ bifurcation analysis to take a closer look at the transitions.

For large viscosity an equilibrium state is the global attractor for this system. At $\nu \approx 0.0113$ a Hopf bifurcation occurs in which a stable periodic orbit is created. To get a first impression of the transitions from periodicity to chaotic and turbulent motion we computed a limit point diagram in the range $0.01 > \nu > 0.004$ of the Poincare map on the plane given by $\tilde{\omega}(0, 2, 4) = 0.005$. The integration time was $\Delta t = 1000$ for each parameter value, after a transient time of 100 time units, using the last point at the previous viscosity as initial value. The limit point diagram is shown in figure (4). Two parameter ranges with periodic behaviour can be seen: one for $\nu > 0.0105$ and one around $\nu = 0.0068$. A continuation of these periodic orbits in parameter ν is shown in figure (5). The branch which is stable

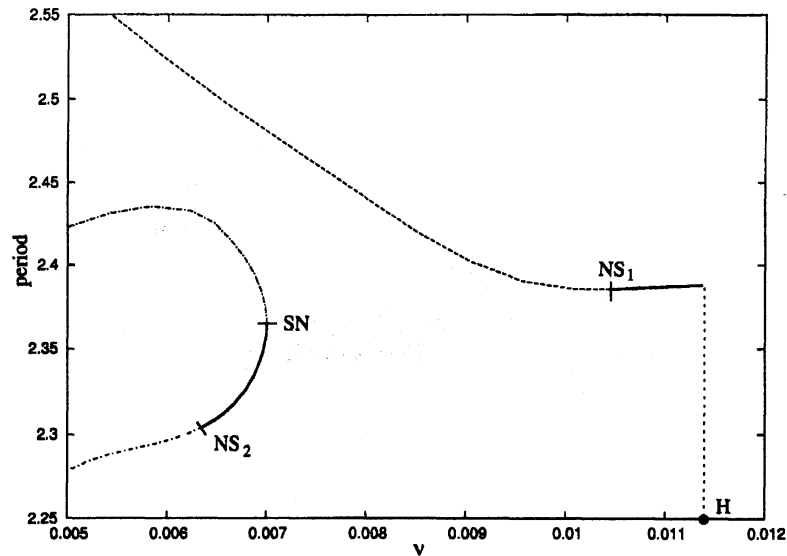


Figure 5: Continuation of two branches of periodic solutions, one created in Hopf bifurcation H and one not connected to a branch of equilibria. Period versus viscosity. Thick lines denote stable orbits, thin lines unstable orbits. SN denotes a saddle-node bifurcation and NS a Neimark-Sacker (torus) bifurcation.

around $\nu = 0.0068$ does not bifurcate from an equilibrium. Both branches become unstable in a Neimark-Sacker, or Torus bifurcation. Directly beyond these bifurcation points we expect the behaviour to be quasi periodic, and indeed invariant circles appear in the Poincare section, figure (4). The transitions which occur near bifurcation points NS_1 and NS_2 are different and lead to different behaviour. In the following sections we will describe the breakdown of the invariant tori in more detail.

4.1 The first transition to chaos: torus doubling bifurcations

As can be seen in figure (4) quasi periodic motion persists over a large parameter range to the left of bifurcation point NS_1 . Theoretically we can expect the quasi periodic behaviour to persist on a fractal domain in parameter space, as proven in Broer *et al.* (1990)(part I). Therefore we might see many transitions. Indeed, to the left of NS_1 we find periodic (phase-locked) motion, 3-periodic motion (as reported on in Kida *et al.* (1989)) and chaos. Transitions between these regimes can be related to bifurcations of phase-locked orbits, as shown in Broer *et al.* (1998), or rather to bifurcations of the torus itself. In Broer *et al.* (1990)(part II) a partial theory of bifurcating tori is developed. In particular quasi periodic saddle-node, period doubling and Hopf bifurcations are shown to occur generically if one parameter is varied. The quasi periodic Hopf bifurcation corresponds to a transition to 3-periodic motion, whereas the quasi periodic period doubling (or torus doubling) results either in two new, disjunct tori or in one new torus with one period doubled. The latter bifurcation shows up in our system.

The first transition from quasi periodic to chaotic is shown in figure (6). The torus doubles at least three times before a chaotic attractor shows up. Cascades of torus dou-

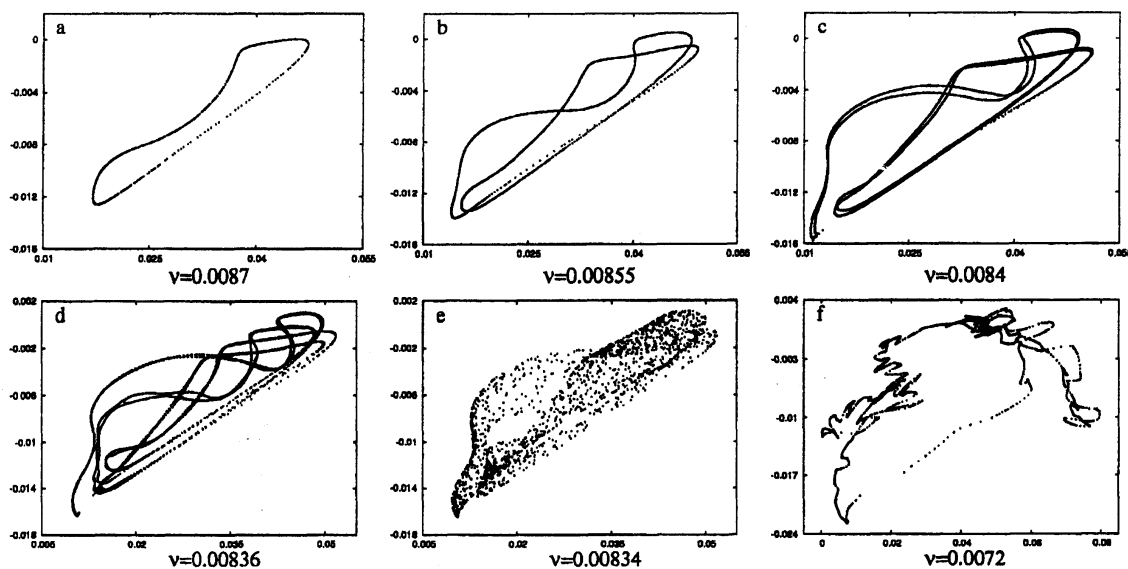


Figure 6: Poincaré sections near bifurcation point NS_1 . Integration time for each picture was $O(10^3)$. From a to d the invariant torus doubles three times whereas the motion remains quasi periodic. At $\nu = 0.00834$, picture e, the motion has become chaotic. Reducing the viscosity further the torus reappears. In picture f it seems to be near breakdown.

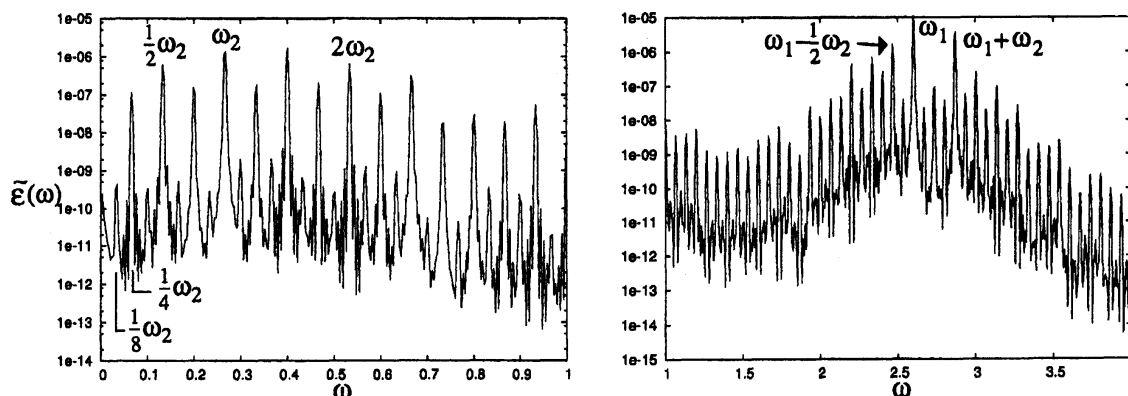


Figure 7: Energy spectrum obtained from an integration with $\nu = 0.00834$ and $\Delta t = 4 \cdot 10^3$. On the left: low frequency domain with fundamental frequency ω_2 and harmonics $\omega_2/2^k$. On the right: high frequency domain with fundamental frequency ω_1 and some combination peaks.

blings were reported on long before the normal form theory was developed, e.g. Kaneko (1983); Franceschini (1983); Anishenko (1990). In spite of attempts to develop scaling and normal form theory, as in Kaneko (1984); Arnéodo *et al.* (1983), those studies were mainly phenomenological and led to the conjecture that, in contrast to doubling cascades of periodic orbits, only a finite number of torus doubling can occur before the torus is destroyed and chaos ensues.

In figure (7) the period doubling the energy power spectrum is shown at parameter

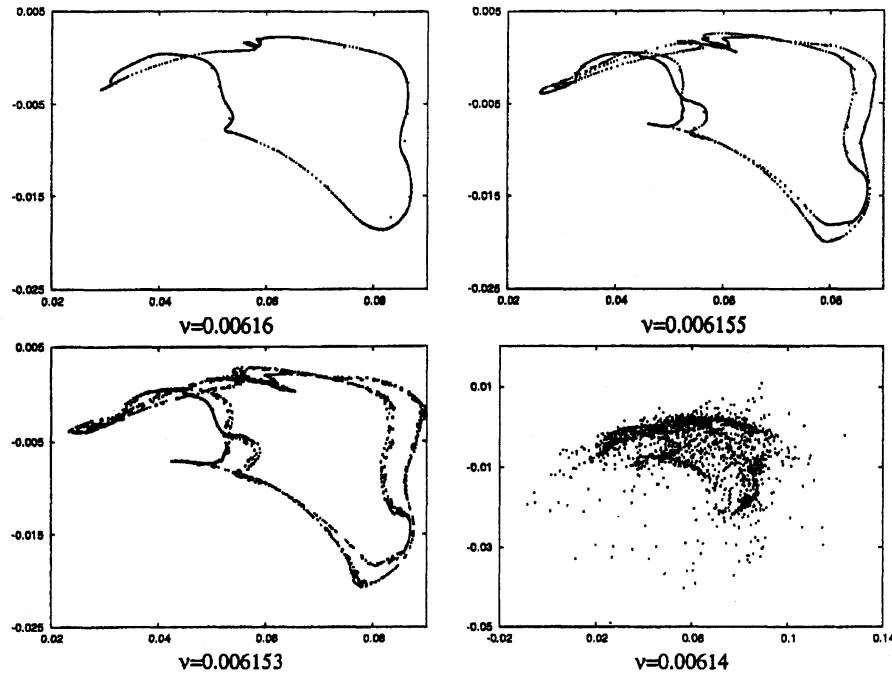


Figure 8: Poincaré sections near bifurcation point NS_2 . Integration time for each picture was $O(10^3)$. From a to b we see the invariant circle double once but in c a third fundamental frequency has appeared in a quasi periodic Hopf bifurcation. In picture d the three periodic motion has broken down and chaos is observed. Note, that the scales have been adjusted.

value $\nu = 0.00836$, corresponding to Poincaré section (6d). Frequency ω_1 lies close to the period of the orbit that is stable for $\nu > 0.0105$. In the low frequency range the other fundamental frequency, ω_2 is shown. The peaks at $\omega_2/2^k$ for $k = 1, 2, 3$ are due to the repeated period doubling. These harmonics also show up in combination peaks, as shown around ω_1 .

4.2 The second transition to chaos: quasi periodic Hopf bifurcation

Stable quasi periodic motion is again found beyond bifurcation point NS_2 (see figure (5)). The corresponding invariant circle of the Poincaré map is shown in figure (8a). If we decrease the viscosity we first observe a torus doubling as described above. The double invariant circle is shown in figure (8b). However, subsequent doubling bifurcations are not found. Instead for slightly lower viscosity we find three periodic motion. A quasi periodic Hopf bifurcation has occurred and a third fundamental frequency has been created. The three dimensional torus shows up in the Poincaré section as a thick invariant circle, see figure (8c). As was shown by Ruelle & Takens (1971) the three periodic motion is unstable to perturbations and if we decrease viscosity further a chaotic attractor shows up (8d). Thus, the second transition to chaos follows a scenario different from the first one.

The energy spectrum for three periodic motion is shown in figure (9). The first fundamental frequency, ω_1 , is again related to the period of the orbit from which the torus bifurcates. The second fundamental frequency, ω_2 , has an associated peak, albeit rather

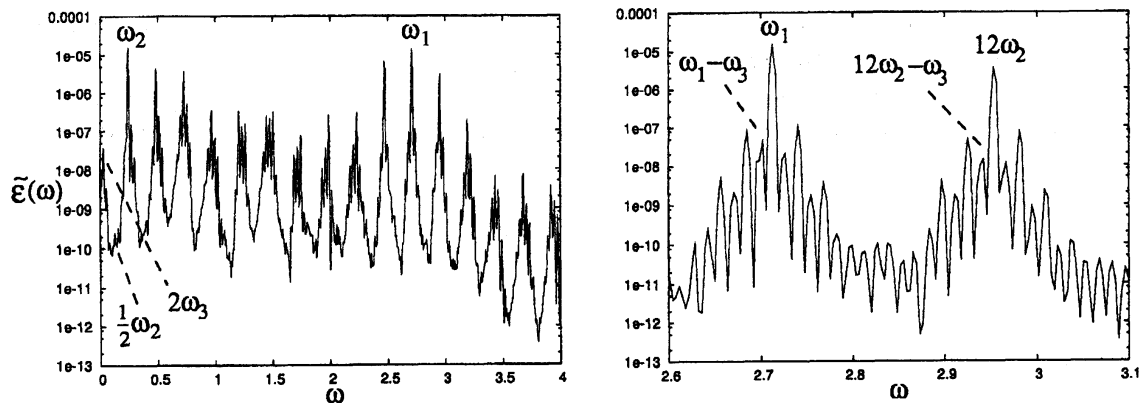


Figure 9: Energy spectrum obtained from an integration with $\nu = 0.00834$ and $\Delta t = 4 \cdot 10^3$. On the left: low frequency domain with fundamental frequency ω_2 and harmonics $\omega_2/2^k$. On the right: high frequency domain with fundamental frequency ω_1 and some combination peaks.

weak, at $\omega_2/2$ due to the doubling bifurcation. The third fundamental frequency, ω_3 , is fairly small but we can see its harmonics. On the right hand side an enlargement around ω_1 is shown. The system is near 1 : 11 resonance so that the peaks at $11\omega_2$ and ω_1 almost coincide. Combination peaks with the third fundamental frequency are shown around ω_1 and $12\omega_2$.

5 Conclusion

Taking full advantage of the symmetries and divergence free condition we have simulated high symmetric flow at micro scale Reynolds numbers in the range $R_\lambda \approx 27 - 55$. As reported in Kida *et al.* (1989), we see intervals with stable periodic motion in this range, followed by a transition to quasi periodic and, subsequently, chaotic motion for decreasing viscosity. By the use of bifurcation analysis, Poincaré sections and power spectra we have shown that these transitions are different in nature. The first transition to chaos is due to a sequence of torus doubling bifurcations. The theory of such cascades is as yet incomplete and scaling laws similar to those for doubling cascades of periodic orbits haven't been derived. The impression from numerical simulations and experiments is that only a finite number of torus doublings can occur before chaos ensues (Arnéodo *et al.*, 1983; Anishenko, 1990). In our system we observe three doublings, but further integrations might reveal more doubling bifurcations, which would contribute to the formulation of scaling laws.

If we decrease viscosity beyond the first transition point we find an interval in parameter space with many transition between periodic, quasi periodic and chaotic motion. This is in agreement with the theory formulated by Broer *et al.* (1990), which says that quasi periodic motion will be stable on a fractal set in parameter space. In this region the spatial structure of the flow remains simple and only large scale vortices arise.

The second transition is shown to follow the Ruelle-Taken (1971) scenario, periodic \rightarrow two-periodic \rightarrow three-periodic \rightarrow chaotic. Poincaré sections show that a chaotic attractor is created which is large compared to the three dimensional torus destroyed in the transition

process. This attractor persists for decreasing viscosity as the micro scale Reynolds number exceeds 50 and turbulent motion sets in.

The difference in behaviour beyond the transition points through quasi periodic doubling and quasi periodic Hopf bifurcations leads to the hypothesis that quasi periodic doubling might induce temporal chaos but not turbulence, whereas the quasi periodic Hopf bifurcation, introducing an extra fundamental frequency, can lead to turbulent motion.

In future work continuation of periodic orbits to low viscosity will be performed, hoping to find periodic orbits embedded in the turbulent attractor.

6 Acknowledgments

I would like to thank the National Institute for Fusion Science in Toki, Japan, for the time I spent working there, Shigeo Kida, Genta Kawahara, Henk Broer and Eusebius Doedel for useful discussions and Greg Lewis for his hospitality at the University of Ontario Institute of Technology. This work was supported by the Japan Society for Promotion of Science.

References

- ANISHENKO, V.S. 1990. *Complex oscillations in simple systems*. Nauka, Moscow.
- ARNÉODO, A., COULLET, P.H., & SPIEGEL, E.A. 1983. Cascade of period doublings of tori. *Phys. Lett. A*, **94**, 1–6.
- BROER, H. W., SIMÓ, C., & TATJER, J. C. 1998. Towards global models near homoclinic tangencies of dissipative diffeomorphisms. *Nonlinearity*, **11**, 667–770.
- BROER, H.W., G.B., HUITEMA, TAKENS, F., & BRAAKSMA, B.L.J. 1990. Unfoldings and bifurcations of quasi-periodic tori. *Mem. AMS*, **83**(421).
- DOEDEL, E. 2003. Private communications.
- DOEDEL, E., CHAMPNEYS, A., FAIRGRIEVE, T., KUZNETSOV, YU. A., SANDSTED, B., & WANG, X.J. 1986. *AUTO97: Continuation and bifurcation software for ordinary differential equations (with HomCont)*. Computer Science, Concordia University, Montreal, Canada.
- FRANCESCHINI, V. 1983. Bifurcations of tori and phase locking in a dissipative system of differential equations. *Physica D*, **6**, 285–304.
- KANEKO, K. 1983. Doubling of torus. *Prog. Theor. Phys.*, **69**, 1806–1810.
- KANEKO, K. 1984. Oscillation and doubling of torus. *Prog. Theor. Phys.*, **72**, 202–215.
- KIDA, S. 1985. Three-dimensional periodic flows with high-symmetry. *J. Phys. Soc. Japan*, **54**(6), 2132–2136.
- KIDA, S., & MURAKAMI, Y. 1989. Statistics of velocity gradients in turbulence at moderate Reynolds number. *Fluid.Dyn.Res.*, **4**, 347–370.

- KIDA, S., YAMADA, M., & OHKITANI, K. 1989. A route to chaos and turbulence. *Physica D*, **37**, 116–125.
- RUELLE, D., & TAKENS, F. 1971. On the nature of turbulence. *Commun. math. Phys.*, **20**, 167–192.
- TUWANKOTTA, J. M., & QUISPEL, G. R. W. 2003. Geometric numerical integration applied to the elastic pendulum at higher-order resonance. *J. Comput. Appl. Math.*, **154**, 229–242.